

Simulations of Computing by Self-Assembly

Erik Winfree
California Institute of Technology
winfree@hope.caltech.edu

May 31, 1998

Abstract Winfree (1996) proposed a Turing-universal model of DNA self-assembly. In this abstract model, DNA double-crossover molecules self-assemble to form an algorithmically-patterned two-dimensional lattice. Here, we develop a more realistic model based on the thermodynamics and kinetics of oligonucleotide hybridization. Using a computer simulation, we investigate what physical factors influence the error rates, i.e., when the more realistic model deviates from the ideal of the abstract model. We find, in agreement with rules of thumb for crystal growth, that the lowest error rates occur at the melting temperature when crystal growth is slowest, and that error rates can be made arbitrarily low by decreasing concentration and increasing binding strengths.

1 Introduction

Early work in DNA computing (Adleman 1994; Lipton 1995; Boneh et al. 1996; Ouyang et al. 1997) showed how computations can be accomplished by first creating a combinatorial library of DNA and then, through successive application of standard molecular biology techniques, filtering the library to identify the DNA representing the answer to the mathematical question. In these approaches, the problem to be solved determines the sequence of laboratory operations to be performed; the length of this sequence grows with problem size, intimidating many experimental researchers. Consequently, a few researchers have begun looking into chemical systems capable of performing many logical steps in a single reaction, thus leading to paradigms for DNA computing where the problem to be solved is encoded strictly in DNA sequence; a fixed sequence of laboratory operations is performed to determine the answer to the posed question. Promising approaches include techniques based on PCR-like reactions (Hagiya et al. in press; Sakamoto et al. in press; Hartemink and Gifford in press; Winfree in press) and techniques based on DNA self-assembly (Winfree 1996; Winfree et al. in press; Jonoska et al. in press). Although there has been experimental work exploring all these models, typically only a few logical operations have been demonstrated. It is at this point unclear how well any of the techniques can be scaled up. Short of full experimental demonstration, realistic simulations of the chemical kinetics and thermodynamics can shed light on what can be expected of these

systems, and can point to parameter regimes where the experiments are most likely to succeed. This paper presents a preliminary analysis of the self-assembly model of Winfree (1996).

To motivate the self-assembly model, we consider the physical process of crystallization. During crystal growth, monomer units are added one-by-one at well-defined sites on the surface of the crystal. There may be more than one type of monomer, in which case there may be several different types of binding site, each with affinity for a different monomer; typically a periodic arrangement of units results. The question of whether periodic lattices will *necessarily* result has been studied in mathematics in the context of two-dimensional tilings (Grünbaum and Shephard 1986). A set of geometrical shapes (the *tiles*) are said to tile the plane if the tiles can be arranged, non-overlapping, such that every point in the plane is covered. A surprising result in the theory of tilings is that there exist sets of tiles which admit *only* aperiodic tilings (Berger 1966; Robinson 1971), the most elegant being the rhombs of Penrose (1978). The variety of aperiodic patterns is limitless: using square tiles with modified edges, the time-space history of any Turing Machine can be reproduced by the tiling pattern¹ (Wang 1963; Robinson 1971). Is it possible to translate these results back to a physical system, to produce aperiodic crystals, or even crystals which “compute”? Already, there is an extensive literature on “quasicrystals” (Steinhardt and Ostlund 1987), materials which exhibit “prohibited” 5-fold symmetry and which are thought to be related to the aperiodic Penrose tiles. The purpose of this paper is to examine the suggestion in Winfree (1996) that DNA double-crossover molecules can be used to make programmable “molecular Wang tiles” that will self-assemble into a 2D sheet to simulate any chosen cellular automaton. It has already been shown experimentally that double-crossover molecules can be designed to assemble into a periodic 2D sheet (Winfree et al. 1998) and that a single logical step can proceed in a model system. In this paper we argue that it is physically plausible to perform Turing-universal computation by crystallization.

2 An Abstract Model of 2D Self-Assembly

The results in the theory of tilings are entirely existential, saying nothing about *how* a correct tiling is to be found. What is missing is a mechanism for producing tilings. In this section we describe the relation of computation and self-assembly by presenting an abstract model of two-dimensional (2D) self-assembly, which we call the Tile Assembly Model. The fundamental units in this model are unit square *tiles* (also called *monomers*) with labelled edges. We have an unlimited supply of tiles of each type. *Aggregates* are formed by placing new tiles next to and aligned with existing ones such that sufficiently many of their edges have matching labels. Tiles cannot be rotated or reflected. To define the model completely, we must be precise about when “sufficiently many” edges match. Each edge label σ_i has an associated *strength* g_i , which must be a non-negative integer. At “temperature” \mathcal{T} , an aggregate of tiles can grow by addition of a monomer whenever the summed strength of matching edges exceeds \mathcal{T} (mismatched labels neither contribute nor interfere) – these are called *stable* additions. We say that a set of tiles P *produces* aggregate A from *seed* tile T if A can be obtained from the single tile T by a sequence

¹Even more is possible: there exist tile sets which produce *non-recursive* patterns (Hanf 1974; Myers 1974)! However, it is unlikely that any physical process could give rise to non-recursive patterns, in any computable amount of time. All models discussed in this paper are strictly computable.

of zero or more stable additions of monomers; in which case, we also say simply that P produces A (if there is no need to specify the seed tile).

To illustrate this model, consider the 7 tiles shown in Figure 1d. The four tiles on the left are called the *rule tiles* because they encode addition mod 2; the three tiles on the right are the *boundary tiles*; the one with two strength-2 edges is the *corner tile*. There are 4 edge labels, of strengths 0, 1, 1, and 2. At temperature $\mathcal{T} = 0$, every possible monomer addition is stable, and thus random aggregates are produced. At temperature $\mathcal{T} = 1$, at least one edge must match for an addition to be stable, but now the arrangement of tiles within an aggregate depends upon the sequence of additions. At temperature $\mathcal{T} = 2$, there is a unique choice for the tile in each position relative to the corner tile, independent of the sequence of events. Under these conditions, this set of tiles produces the Sierpinski Triangle by computing Pascal's Triangle mod 2. At temperature $\mathcal{T} = 3$, no aggregates are produced because no monomer addition to another monomer is stable.

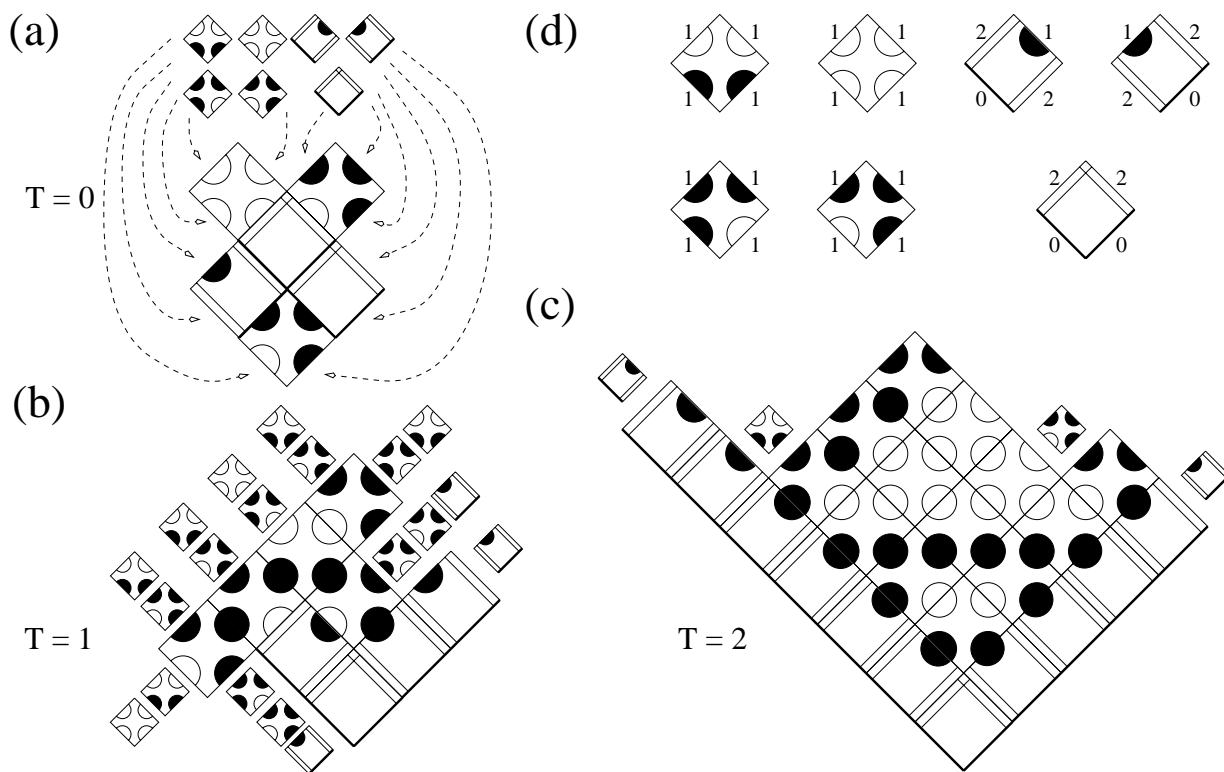


Figure 1: The Sierpinski Tile set is shown in (d). The strengths of edges are marked, and the edge labels are denoted graphically. In (a) - (c), small tiles are used to indicate possible stable additions to the aggregate. (a) When $\mathcal{T} = 0$, any tile addition is stable, and a random aggregate results. (b) When $\mathcal{T} = 1$, typically several stable possibilities at each site; again, a random aggregate results. (c) When $\mathcal{T} = 2$, there is a unique possibility at each site, resulting in unique pattern formation.

Whereas it is impossible to uniquely produce non-trivial aggregates when $\mathcal{T} = 0$, an arbitrary shape can be produced at $\mathcal{T} = 1$ by assigning a unique tile to each position and giving each edge a unique label. However, this requires the use of many tiles. At $\mathcal{T} = 2$ we can produce interesting patterns with few tiles.

A hint of the computational power of the Tile Assembly Model when $\mathcal{T} = 2$ is provided by a simulation of cellular automata². The proof we develop below demonstrates two important points. First, even though tile addition is stochastic, a unique pattern is produced regardless of the order of events, because only stable tile additions are made. Second, the arrangement of tile types on the 1D growth front of the aggregate can represent information (much like how the arrangement of 0's and 1's on a 1D tape represents information for a Turing Machine), and stable tile additions can modify that information by specified rewrite rules, resulting in fully general computation.

Our simulation is based on one-dimensional blocked cellular automata (BCA)³, a variety of cellular automaton (CA). It is known that BCA and CA are Turing-universal models, and simple simulations of Turing machines have been demonstrated (Smith 1971; Biafore preprint). We begin by defining BCA.

Definition: A k -symbol BCA is defined (using the integers $\{1, 2, \dots, k\} = \mathcal{Z}_k$) by a rule table

$$R = \{(l_i, r_i) \rightarrow (l'_i, r'_i)\} \subset (\mathcal{Z}_k \times \mathcal{Z}_k \rightarrow \mathcal{Z}_k \times \mathcal{Z}_k).$$

If R is a function, then the BCA is termed deterministic. The *state* \mathbf{c} of the BCA assigns a symbol to every location on an infinite linear array of *cells*. At each time step every cell in \mathbf{c}^t is rewritten to produce \mathbf{c}^{t+1} ; thus we use $c^t(x)$ to denote the symbols written in cell x after t steps. The BCA uses R to re-write pairs of cells in \mathbf{c} , alternating between even and odd alignments of the pairing: for even t and even x , and for odd t and odd x ,

$$\left((c^t(x), c^t(x+1)) \rightarrow (c^{t+1}(x), c^{t+1}(x+1)) \right) \in R.$$

An input to a BCA computation is a state \mathbf{c}^0 with a finite number of non-zero cells. For convenience and without loss of generality, we will confine our attention to n -bit binary inputs \mathbf{b} , and write $\mathbf{c}^0 = \mathbf{b}$ to refer to an input where $c^0(i) = b_i$ for $1 \leq i \leq n$ and $c^0(i) = 0$ otherwise.

The computation of the BCA defines $c^t(x)$ over the half-plane $t \geq 0$. We will show how to construct a set of tiles P such that in all aggregates produced from the seed tile T_0 , if there is a tile at position (i, j) with respect to the seed tile, then the tile has edges encoding $c^{i+j}(i-j)$ and $c^{i+j}(i-j+1)$. Thus the time-history of the BCA computation is reproduced exactly in the self-assembled tile aggregate.

First we show, for any n -bit BCA input \mathbf{b} , how to generate the set of $n+3$ *input tiles* $I(\mathbf{b})$. Figure 2a shows the construction. Because the only edge matches possible with these tiles are strength 2, at $\mathcal{T} = 2$ all produced aggregates are essentially as shown, with variable length regions encoding “zero” on either side. The tile whose top edges encode bits b_1 and b_2 is referred

²This result, presented in less detail in Winfree (1996), translates Wang’s simulation of Turing Machine execution by the Tiling Problem (Wang 1963) into the Tile Assembly Model given here. The Tiling Problem can be viewed as asking for the ground state of an N -state Ising model, which can be seen as a question of equilibrium thermodynamics in the limit as $T \rightarrow 0$. Not only can Ising models be produced which are Turing-universal because the ground state reproduces the space-time history of any chosen Turing Machine, but the proof that tiles sets can be found which tile the plane non-recursively shows in fact that the ground state of an Ising model can be non-recursive. Thus it is essential to study a kinetic, rather than thermodynamic, model.

³BCA are also known as *partitioning* CA (Margolus 1984) (a generalization of lattice gas models), as 2-body CA Biafore (preprint), and by a number of other names.

to as the seed tile T_0 and is used as the reference for indexing tiles by location. The bottom of each input aggregate contains only strength-0 edges, so no further additions can occur there. The top of each input aggregate contains exclusively strength-1 edges, arranged in a zig-zag to form a series of binding sites, called *slots*, where a new tile could make contact with *two* strength-1 edges. For aggregates containing the seed tile T_0 , these edges encode the input \mathbf{c}_0 as well as the odd-even pairing of cells.

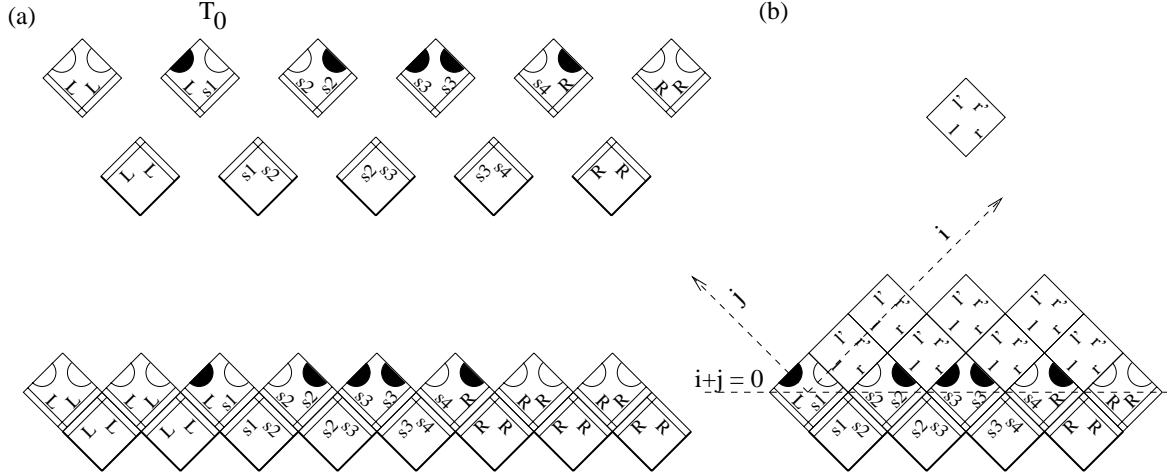


Figure 2: Using the Tile Assembly Model to simulating a BCA computing from a binary input. (a) Input tiles $I(\mathbf{b})$ for $\mathbf{b} = 10011101$, and an aggregate they produce at $\mathcal{T} = 2$. Here we use conventions similar to Figure 1 to indicate the strength of edges: thick edges are strength-0, doubled edges are strength-2, and all other edges are strength-1. (b) Schematic showing a rule tile generated from the BCA rule $(l, r) \rightarrow (l', r')$, and an aggregate produced by the rule tiles and input tiles. Note the dotted lines indicating the default coordinate system with origin at the seed tile T_0 . In this schematic, the edge labels for the rule tiles are not identified.

Next, for BCA rules R we generate a set P_R of k^2 tiles as shown in Figure 2b, using one tile for each rule $(l, r) \rightarrow (l', r')$. All of these *rule tiles* have exclusively strength-1 edges, so at $\mathcal{T} = 2$ they cannot form aggregates with themselves; they must be seeded by the input tiles. Thus, when the tile sets P_R and $I(\mathbf{b})$ are mixed, rule tiles can sit down in the slots presented by the input aggregates iff both of the presented edges match. Consider an aggregate in which: (1) only rule tiles are present above $i + j = 0$, and (2) every rule tile has both of its lower edges correctly matched. It follows directly from the definitions that the edges presented by the tile at (i, j) has edges encoding $c^{i+j}(i - j)$ and $c^{i+j}(i - j + 1)$ because this is true of the input tiles, and every rule tile respects the update rule for the BCA. What remains to be shown is that (1) and (2) hold for every aggregate produced at $\mathcal{T} = 2$. This is done by induction on N , the number of rule tiles in an aggregate. For convenience, we refer to an aggregate containing exactly N rule tiles as an N -aggregate.

Base case: (1) and (2) hold for any 0-aggregate.

Induction: Assume (1) and (2) hold for all N -aggregates. Note that (1) and (2) together imply that above $i + j = 0$, the exposed edges of the aggregate are all *upper* edges. Any $(N + 1)$ -aggregate must be produced from an N -aggregate by a sequence of stable additions of input tiles followed by a stable addition of a rule tile. (1) holds for the new aggregate because all

exposed edges above $i + j = 0$ are upper edges labelled from \mathcal{Z}_k , while all lower edges of input tiles are labelled from $\{L, R, s_1, \dots, s_n\}$. (2) holds for the new aggregate because a rule tile must match two edges to be added, and only upper edges are presented, so the rule tile’s two lower edges must match. \square

Thus, we have proven:

Theorem: Let R be a BCA, and let $c(t, x)$ be the value of cell x at time t for a computation on input \mathbf{b} . If an aggregate produced from seed T_0 by the tile set $P = P_R \cup I(\mathbf{b})$ has a tile in position (i, j) , then the tile’s upper edges encode $c^{i+j}(i - j)$ and $c^{i+j}(i - j + 1)$.

In other words, the Tile Assembly Model uses asynchronous and self-timed updates to simulate any deterministic one-dimensional BCA. Similar arguments can be used to show that the Tile Assembly Model can simulate any *non-deterministic* one-dimensional BCA, in the sense that every possible aggregate produced according to the Tile Assembly Model will represent a possible history of execution of the non-deterministic BCA. In this case, R will contain rules with identical left-hand sides, and consequently in some slots multiple rule tiles will match both exposed edges; thus a non-deterministic choice must be made. Alternatively, a non-deterministic set of input tiles may be used to generate a combinatorial set of possible input strings, followed by deterministic evaluation of each input. The potential for non-determinism is important for using self-assembly to solve combinatorial search problems in the spirit of Adleman (1994).

3 Implementation by Self-Assembly of DNA

We follow Winfree (1996) in developing a molecular implementation of the Tile Assembly Model: each tile is represented by a DNA double-crossover (DX) molecule (Fu and Seeman 1993) with four sticky ends whose sequences represent the edge labels. We would like these molecular “tiles” to self-assemble into a two-dimensional sheet according to the rules of the Tile Assembly Model (see Figure 3). Thus, we need to show:

1. Double-crossover molecules can be designed to self-assemble into two-dimensional crystal lattices – in preference over, for example, random tangled nets, tubes, or other structures. This has in fact now been demonstrated in an experimental system (Winfree et al. 1998).
2. The strengths of edge labels in the model can be implemented by designing the sticky end sequences with specific energetics of hybridization. The DNA hybridization strengths depend primarily on the number of base pairs, with adjustments for their particular sequence, the buffer conditions, and temperature. Thus, for example, longer sticky ends can be used to represent edge labels with greater strength.
3. The binding of DX molecules into slots, where two sticky end sequences must both hybridize, is *cooperative* – thus, strengths “add”. We will argue below that this is *a priori* likely; furthermore, suggestive experimental evidence has been presented in Winfree et al. (in press).

4. There is a physical parameter analogous to \mathcal{T} which determines the strength required for association of molecular tiles. This parameter can be, for example, the temperature T . DNA sticky ends bind more strongly at low temperatures, and conversely, at higher temperatures more sticky-end interactions will be necessary for stable addition.
5. All these considerations can come together to produce molecular self-assembly in accordance with the Tile Assembly Model.

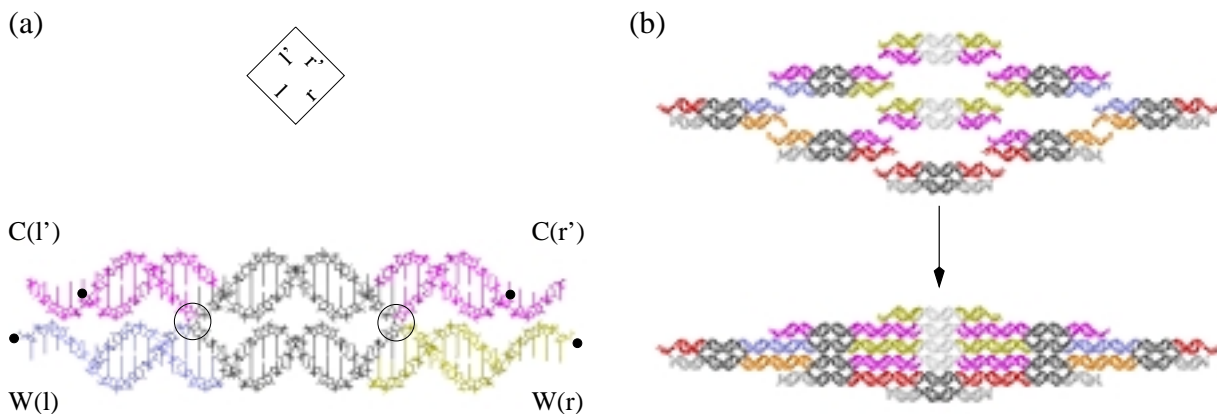


Figure 3: The DNA representation of Wang tiles. (a) A molecular Wang tile (double crossover molecule) representing the rule $(l, r) \rightarrow (l', r')$. The molecule consists of an interior structural region and four double-stranded arms, each terminated by a single-stranded sticky end. Edge labels are implemented using unique sticky-end sequences. Note that sticky-ends for the lower edges use Watson-sense sequences for each label, while the upper edges use the complementary Crick-sense sequences. This ensures the proper relative orientation of tiles. As shown, the same molecule represents both a Wang tile and its reflection about the vertical axis; however, using four encodings for each label ($W_{left}, W_{right}, C_{left}, C_{right}$) eliminates reflection-sense binding. In the double crossover molecule, the crossover points are circled, and dots are placed at the 5' ends of each strand. Color is used to indicate the edge label being represented, and not the identity of strands (each strand is multi-colored). (b) The self-assembly of 9 molecular Wang tiles, of 5 distinct types. These correspond to the 9 tiles at the bottom of Figure 1c. Note that the corner and boundary molecules have hairpin sequences, and thus no sticky ends, on certain of their lower arms; this implements a tile with strength-0 labels on its lower edges. Also note that on the corner and boundary molecules, the red and orange sticky ends are sufficiently longer than the sticky ends on the rule molecules to implement a strength-2 interaction.

Our approach for arguing these points is based on the study of the thermodynamics and kinetics of DNA oligonucleotide hybridization (Wetmur 1991). We review here the elements of this theory that are needed for our discussion.

Let $ssDNA_1$ and $ssDNA_2$ be two Watson-Crick complementary oligonucleotides, and let $dsDNA$ be the double-stranded helical complex that results upon their hybridization. The reaction can be modelled as a two-state first-order system:



We can write a differential equation for the rates of change of the concentration of each species. The units for k_r are 1/sec, so k_r [dsDNA] gives the rate in M/sec of dissociation of the double helix; the units for k_f are 1/M/sec, so k_f [ssDNA₁][ssDNA₂] gives the rate in M/sec of hybridization to form new double helical molecules. Altogether, we have:

$$-[\text{dsDNA}] = [\text{ssDNA}_1] = [\text{ssDNA}_2] = k_r [\text{dsDNA}] - k_f [\text{ssDNA}_1][\text{ssDNA}_2]$$

The rate constants k_f and k_r can be estimated from the DNA sequence and the temperature T (in K), assuming the reaction is taking place in a standard buffer. For very short oligonucleotides, the forward reaction has a diffusion-controlled rate-determining step (Quartin and Wetmur 1989) approximately independent of oligo length and sequence, so:

$$k_f = A_f e^{-E_f/RT} \approx 6 \times 10^5 \text{ /M/sec},$$

where $A_f = 5 \times 10^8 \text{ /M/sec}$ and $E_f = 4 \text{ kcal/mol}$ is the activation energy for the reaction⁴. The reverse rate, on the other hand, is very sensitive to oligo length and sequence:

$$k_r = k_f e^{\Delta G_s^\circ/RT},$$

where $R = 2 \text{ cal/mol/K}$ and $\Delta G_s^\circ < 0$ is the free energy released as heat by a single hybridization event⁵. The standard free energy ΔG_s° can be calculated from the standard enthalpy ΔH_s° and the standard entropy ΔS_s° of the reaction: $\Delta G_s^\circ = \Delta H_s^\circ - T\Delta S_s^\circ$. For reactions taking place in commonly used buffers, the standard enthalpy and entropy can be reliably estimated from the sequence according to a nearest-neighbor model (SantaLucia et al. 1996); however, for the purposes of this discussion, we can use the coarser approximation for length- s oligonucleotides⁶: $\Delta H_s^\circ \approx -8s \text{ kcal/mol}$ and $\Delta S_s^\circ \approx -22s - 6 \text{ cal/mol/K}$. Thus we can predict both k_f and k_r for the hybridization of complementary oligonucleotides. This allows us to predict the equilibrium concentrations of each species via the equilibrium constant

$$K \doteq \frac{[\text{dsDNA}]}{[\text{ssDNA}_1][\text{ssDNA}_2]} = \frac{k_f}{k_r} = e^{-\Delta G_s^\circ/RT}.$$

We will use our understanding of oligonucleotide hybridization kinetics and thermodynamics to build a plausible model for the self-assembly of DX molecules via the hybridization of their sticky ends.

⁴We will ignore the activation energy in what follows, because we will see that the value of k_f has no effect on the behavior of the system except to set the scale of the time axis.

⁵The more negative ΔG_s° is, the more heat is released upon association and the more favorable the reaction is. Another way of looking at it is that if ΔG_s° is very negative, a lot of heat must simultaneously converge upon a single double helical DNA molecule in order to cause dissociation, and thus dissociation is rare. Also note that here, as elsewhere, $e^{\Delta G_s^\circ/RT}$ has an “invisible” unit of M, so that k_r is in units of 1/sec.

⁶The empirical value $\Delta S_{init} = -6 \text{ cal/mol/K}$ can be considered the entropic cost of aligning the two strands to have the same orientation, and is called the initiation entropy.

4 A Kinetic Model of DNA Self-Assembly

The self-assembly of two-dimensional lattices from a heterogeneous mix of N DX molecules is a far more complicated system than the hybridization of two oligonucleotides. Rather than having just three species to consider (ssDNA₁, ssDNA₂, and dsDNA), we now have an infinite number of species (all possible aggregates). For each aggregate of n tiles with m available sites, there are Nm association reactions and n dissociation reactions. Note that at every available site, there is an association reaction for every possible monomer, regardless of whether the monomer is the “correct” one or not; to understand when correct behavior can be expected, we must look closely at the kinetics of all the reactions. The model we develop here can be seen as an extension of Erickson (1980), which considers the self-assembly of an isotropic two-dimensional lattice consisting of a single unit type. To model the kinetics of self-assembly, we make several simplifying assumptions:

1. Monomer concentrations will be held constant. Further, all monomer types will be held at the same concentration. Primarily we make this assumption because the analysis is easier. Later we show how the results found with the assumption can be used to understand the more general case when the assumption is not true⁷.
2. Aggregates do not interact with each other; thus the only reactions to model are the addition of a monomer to an aggregate, and the dissociation of a monomer from an aggregate. Potential drawbacks of this assumption will be discussed at the very end.
3. As in the hybridization of oligonucleotides, we assume that the forward rate constants for all monomers are identical. In particular, the forward rate constants for correct and incorrect additions are identical.
4. As in the hybridization of oligonucleotides, we assume that the reverse rate depends exponentially on the number of base-pair bonds which must be broken, and that mismatched sticky ends make no base-pair bonds. This amounts to assuming that binding on multiple edges is cooperative and that mismatched sticky ends do not affect the dissociation rate in any way.

The model is governed by two free parameters, both of which are dimensionless free energies: $G_{mc} > 0$ measures the entropic cost of fixing the location of a monomer unit (and thus is dependent upon monomer concentration), and $G_{se} > 0$ measures the free energy cost of breaking a single sticky-end bond; both are expressed with respect to the thermal energy RT . A third parameter, the forward rate constant k_f , is immaterial to the behavior of the system; it sets the units for the time axis. The behavior of the system can be understood independently of the exact correspondence of these abstract parameters to more realistic physical parameters; however, we sketch the correspondence below.

⁷There is some intrinsic interest in the case where the assumption is true; for example, biological self-assembly often occurs in the context where genetic circuitry controls the concentration of the monomers via a feedback loop.

For convenience, we lump location, orientation, and other entropic factors together into an “effective concentration” of monomers, $[\hat{\text{DX}}]$. In these units, $[\hat{\text{DX}}] = [\text{DX}]/20$, $\hat{k}_f = 20k_f$, and the initiation entropy of $\Delta S_{init} = -6 \text{ cal/mol/K} = -R \ln 20$ disappears from the equations. Now we write the concentration of each monomer as $[\hat{\text{DX}}] = e^{-G_{mc}}$. Thus the rate of associations of a particular monomer type at a particular site on a particular aggregate is

$$r_f = k_f[\text{DX}] = \hat{k}_f e^{-G_{mc}},$$

measured in 1/sec. To determine the dissociation rate of a unit bound by b sticky-end bonds, each of length s , we will use our assumption of cooperativity to justify using the free energy of a single length- $b \cdot s$ oligonucleotide, $\Delta G_{b,s}^\circ$. To write the dissociation rate in terms of G_{se} , we have:

$$r_{r,b} = k_f e^{\Delta G_{b,s}^\circ/RT} = \hat{k}_f e^{-bG_{se}},$$

also measured in 1/sec. Using the values for ΔH_s° and ΔS_s° determined for oligonucleotide hybridization, sticky ends of length s would correspond to $G_{se} = (\frac{4000 \text{ K}}{T} - 11)s$. If strength-1 edge labels are encoded with sticky ends of length s ($b = 1$), then strength-2 edge labels will be encoded with sticky ends of length $2s$ ($b = 2$). If b is the sum of the strength of all a tile’s matching edges, then the tile’s dissociation rate will be $r_{r,b}$, and we will call b the number of (sticky-end) *bonds*.

The various reactions possible in this model, which we call the Kinetic Assembly Model, are illustrated for the Sierpinski Tiles in Figure 4.

We now wish to understand the behavior of the Kinetic Assembly Model as a function of its two free parameters, G_{mc} (controlled by monomer concentration) and G_{se} (controlled by temperature and by sticky-end length). Our naive prediction is that the ratio $\frac{G_{mc}}{G_{se}}$ plays the role of \mathcal{T} in the Tile Assembly Model. If for small $0 < \epsilon < 1$

$$\mathcal{T} \doteq \frac{G_{mc}}{G_{se}} = b - \epsilon,$$

then for a tile with b matches at a site,

$$\frac{r_f}{r_{r,b}} = e^{bG_{se} - G_{mc}} = e^{\epsilon G_{se}} > 1,$$

and the site will tend to be filled. But a tile with $b - 1$ matches will have

$$\frac{r_f}{r_{r,b}} = e^{-(1-\epsilon)G_{se}} \ll 1,$$

and the tile will tend to dissociate. Because at equilibrium for the local site, the correct tile is preferred over incorrect tiles by a factor of $e^{G_{se}}$, we expect that for large G_{se} , the Kinetic Assembly Model will with high likelihood produce aggregates produced by the Tile Assembly Model. To confirm this expectation and delineate when it applies, we will have to understand when local equilibrium is achieved, when the kinetics works in our favor, and when it works against us.

We begin our detailed analysis by simulating the behavior of the Kinetic Assembly Model. Because there are an infinite number of possible aggregate types, we cannot simply integrate

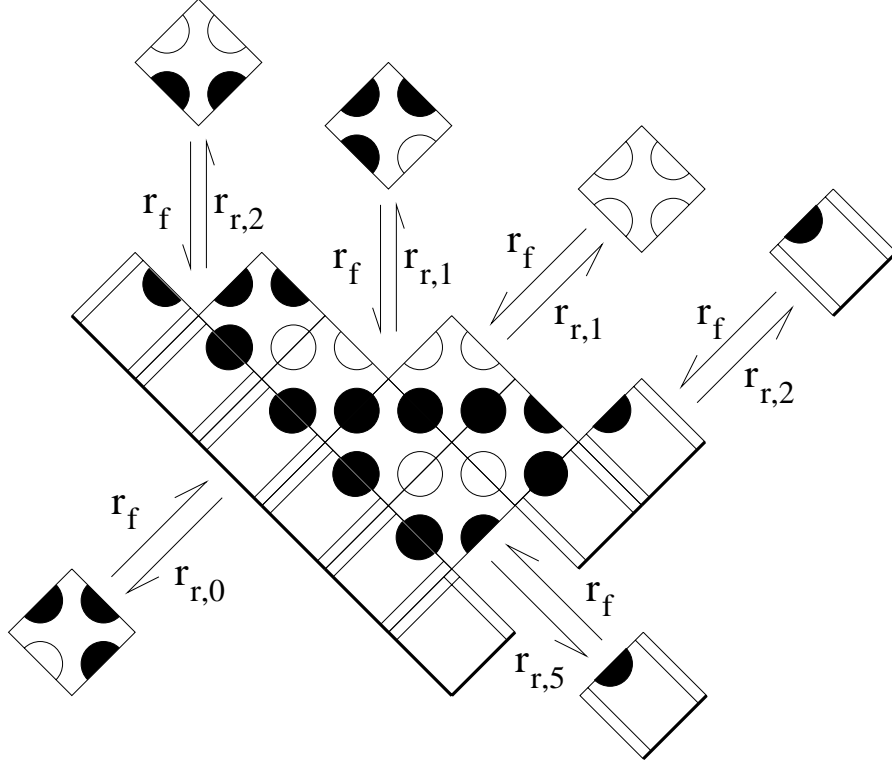


Figure 4: The rates of reactions for various tile association and dissociation steps in the Kinetic Assembly Model. Note that all on-rates are identical, and that off-rates depend only upon the total strength of correct edge matches. Mismatched edges and empty neighbors are treated identically.

the rate equations to determine the time evolution of the concentration of each aggregate type. However, since aggregates do not interact with each other, we can develop our simulation from the perspective of an individual aggregate, starting with a chosen seed unit. Reaction rates now become probability rates for a Poisson process: the association or dissociation of a monomer from the current aggregate. In such a simulation, the probability of observing a particular aggregate at simulated time t corresponds to the fractional concentration of that aggregate at time t according to the full model.

The simulation proceeds as follows: A 2D array is used to store the arrangement of tiles in the current aggregate. Initially the array contains all zeros to indicate empty sites, except for the origin, which contains the seed tile. To determine the next event, the rates of all possible reactions must be known. All m empty sites adjacent to the aggregate are counted; the net on rate is

$$k_{on} = m \hat{k}_f e^{-G_{mc}}.$$

For all occupied sites (i, j) within the aggregate (except for the seed tile at the origin), the tile types of its neighbors are noted and the total strength b_{ij} of all matching labels is calculated; the net off rate is $k_{off} = \sum_b k_{off,b}$ where

$$k_{off,b} = \sum_{ij \text{ s.t. } b_{ij}=b} \hat{k}_f e^{-b_{ij} G_{se}}.$$

Thus the net rate for events of any kind is $k_{any} = k_{on} + k_{off}$, and the time until the next event occurs, Δt , is chosen according to the Boltzman distribution $\Pr(\Delta t) = k_{any}e^{-k_{any}\Delta t}$. Now, given that an event has occurred, the probability that it is an on-event is k_{on}/k_{any} , in which case all sites and all tile types are equally likely to be chosen; otherwise a dissociation has occurred, and the probability that some site with b bonds dissociates is $k_{off,b}/k_{off}$, and again all such sites are equally likely. Once the event is chosen and the array is updated, all rates must be recalculated to determine the next event⁸.

5 Simulation Results

This section discusses simulations of the self-assembly of the Sierpinski Tiles using the Kinetic Assembly Model. An example run is shown in Figure 5. Several features of this simulation run warrant comment.

Shape: The growth front does not advance synchronously, but rather performs a biased random walk, with the following restriction: because stable addition occurs only at concave corner sites (slots) on the growth front, no sites can be more than one step ahead of or behind its neighbors. The growth front is concave on average: the boundary tiles grow fastest because their growth site is always available, while internal regions on the growth front grow slower because stable addition can occur at only a fraction of sites at any given time.

Errors: For the most part, the Sierpinski Triangle is accurately reproduced. However, incorrect tiles do appear. In the first three frames, incorrect tiles can be seen on the border of the aggregate. These are inconsequential errors due to the equal on-rates of all tiles; they will fall off immediately and cause no permanent errors. However, in the last frame we see an incorrect tile which has been embedded within the aggregate; although it has a mismatch with its predecessors, successive tile additions have been correct *with respect to the error*, and now the erroneous tile has 3 matched edges. It has caused a permanent error, and the misinformation spreads to all downstream cells in the computation.

Array Size: In the last two frames, the size of the aggregate has exceeded the size of the array used in the simulation. Thus the Kinetic Assembly Model is not perfectly simulated; a maximal size of aggregate is imposed. In the simulations below, this does not affect the results in the region of interest, but it does explain the constant size (the maximum) found during fast, random aggregation.

To map out the parameter space of this model, simulations of the Sierpinski tiles were performed for all $1 \leq G_{mc}, G_{se} \leq 30$. Each simulation was run for $60/r_f$ simulated seconds, thus on average each unoccupied site could experience up to 60 on-events of each type; consequently, the distribution of aggregate sizes is comparable across different parameter values. Figure 6 shows the results for (a) aggregates seeded by the corner tile and (b) aggregates seeded by a

⁸The actual computer code is optimized to remove redundant calculations, of course!

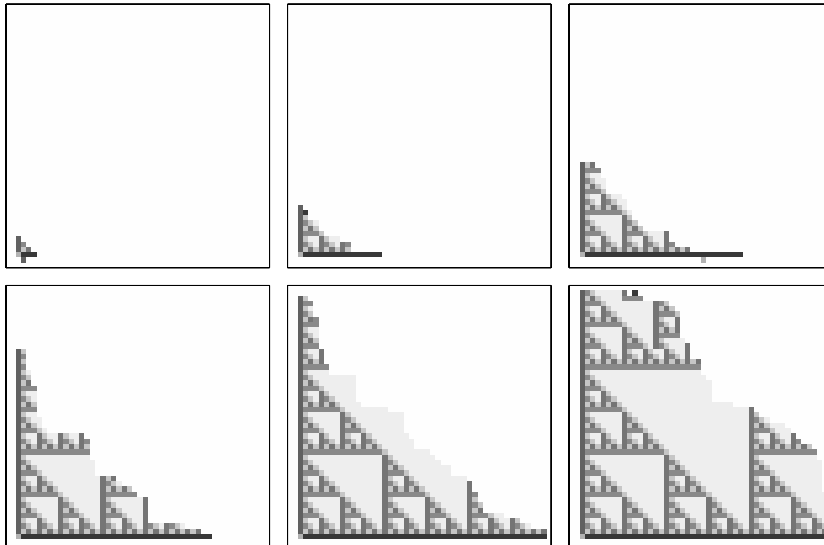


Figure 5: Growth of the Sierpinski Triangle. Greyscale indicates the tile type in the aggregate. The simulation uses parameters $G_{se} = 8$ and $\mathcal{T} = 1.95$, and the seed is a corner tile. These values correspond to monomer concentration of $3 \mu\text{M}$ and $r_f = 2/\text{sec}$, with sticky ends of length 5, and $T = 45^\circ\text{C}$; the frames show growth after 9, 18, 36, 63, 99, and 162 seconds.

rule tile, indicating both the resulting size of the aggregate and the number of errors⁹ in the aggregate.

The lines show $\mathcal{T} = \frac{G_{mc}}{G_{se}} = 2$ and $\mathcal{T} = 1$, which we will respectively call the melting transition and the precipitation boundary. Above the melting transition, no aggregates grow from either seed. Below the precipitation boundary, monomers associate freely to produce random aggregates similar to those produced in the Tile Assembly Model at $\mathcal{T} = 1$. The rate of growth of random aggregates appears to fall off exponentially above the precipitation boundary; this is indicated by the decreasing size of aggregates seeded by a rule tile in (b) and by the decreasing error rate within aggregates seeded by the corner tile in (a). The result is that there is a large region of parameter space where simultaneously (1) growth does occur, (2) errors are rare, and (3) growth *not* initiated by the corner tile does *not* occur¹⁰. We call this *controlled growth*.

We are particularly interested in the behaviour of the Kinetic Assembly Model near the melting transition. Figure 7a shows the size and number of errors as a function of G_{se} , for $G_{mc} = 16$. Upon passing the melting transition ($G_{se} = 8$), the size of aggregates seeded by the corner tile grows dramatically, whereas aggregates seeded by the rule tile do not grow until $G_{se} \approx 12$, at which point all aggregates are overwhelmed with errors. There are a few isolated instances

⁹What’s actually calculated is the number of erroneous (mismatched) bonds, not the number of erroneous (incorrect with respect to their neighbors) tiles; a single misplaced rule tile could be responsible for 4 such mismatched bonds. However, at low error rates these two measures are equivalent. “100%” means 1 mismatched bond per tile; the error rate therefore could exceed 100% for optimally misplaced tiles, but it does not do so in these simulations.

¹⁰Starting with a boundary tile as a seed, growth would occur, but would soon incorporate a corner tile and produce a proper Sierpinski triangle.

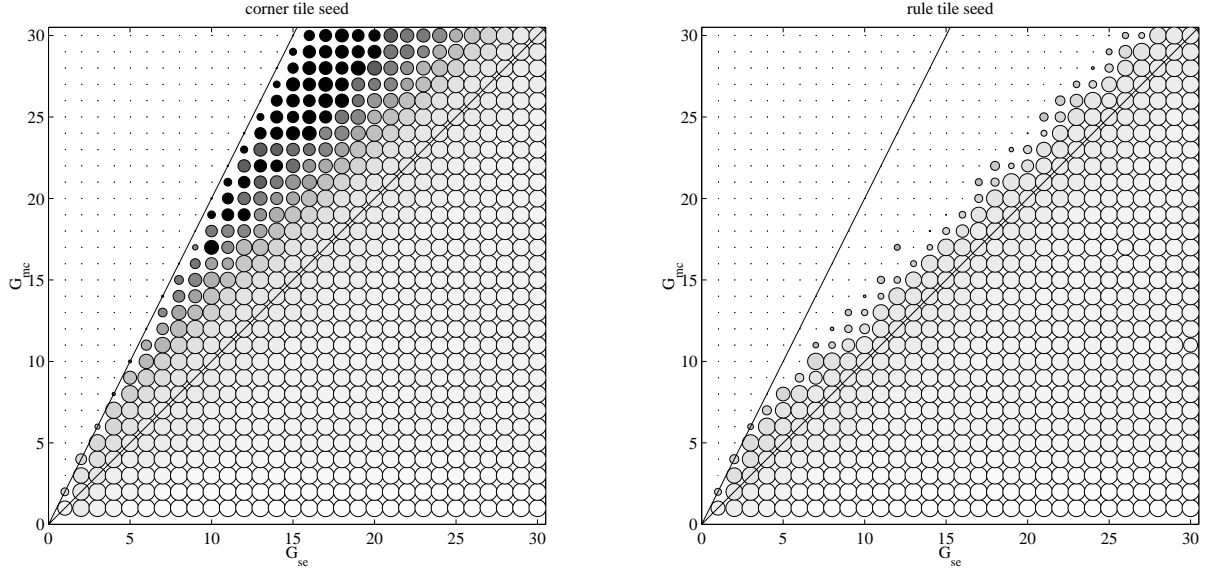


Figure 6: Phase diagrams for the Sierpinski tiles as computed by simulation: (a) aggregates seeded by the corner tile, and (b) aggregates seeded by a rule tile. Each disc represents the results of a single simulation on a 28×28 array; the size of the disc represents the final size of the aggregate, while the shading represents the number of errors as a fraction of total size. Each run was given the same “unitless” time; thus when G_{mc} is high (corresponding to low monomer concentration and thus slow assembly) more time is allowed so that error rates can be compared easily. Solid black indicates zero errors. We see three regimes: $\mathcal{T} > 2$ regime (no growth), $1 < \mathcal{T} < 2$ regime (includes error-free assembly near $\mathcal{T} = 2$), and $\mathcal{T} < 1$ regime (uncontrolled random growth to maximal size). Note that the $\mathcal{T} = 1$ transition is smooth, and hence is not a true phase boundary.

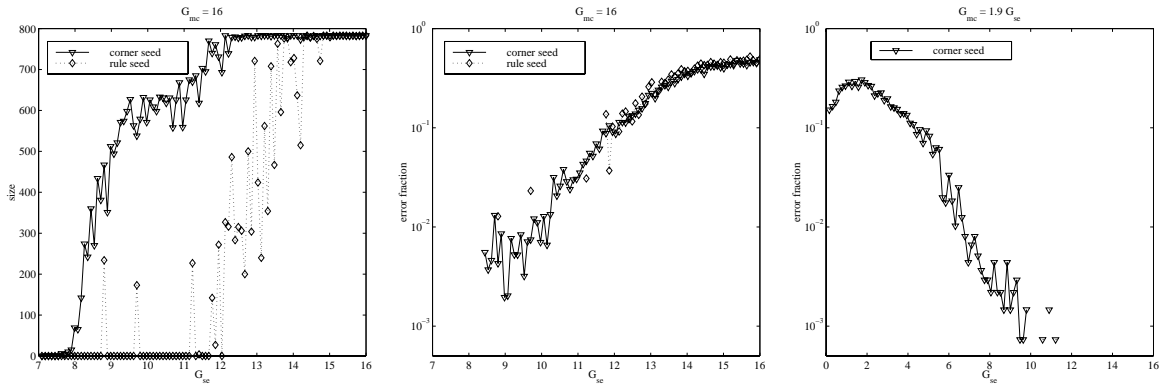


Figure 7: (a) Simulation results for $G_{mc} = 16$ for aggregates seeded with the corner tile and a rule tile. Note that for large G_{se} , where random aggregation is occurring, the aggregate grows to fill the entire 28×28 array. (b) Errors, as a fraction of aggregate size, along the line $G_{mc} = 16$. (c) Errors along the line $\mathcal{T} = 1.9$, using a 38×38 array. Because log axes are used, data points where the aggregate had zero errors are not shown.

where aggregates seeded by the rule tile grow unusually large for G_{se} near 8; in these cases, the aggregate has incorporated a boundary or corner tile, which allows for further growth. Errors appear to decrease exponentially as $G_{se} \rightarrow 8$ (Figure 7b). Figure 7c shows the behavior along $\mathcal{T} = 1.9$, where the system is sufficiently far below the melting transition to grow quickly, and

yet sufficiently close to the melting transition to get low error rates; again, errors appear to fall exponentially with G_{se} .

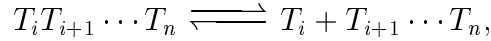
In conclusion, it appears that with probability of error exponentially low in G_{se} , the kinetic model at $\mathcal{T} = 2 - \epsilon$ reproduces¹¹ the Tile Assembly Model at $\mathcal{T} = 2$.

6 Analysis

Equilibrium error rates. We would like to understand why the Kinetic Assembly Model produces these results. We begin by analyzing the equilibrium concentrations for the reaction equations. Consider an aggregate $A = T \cdot A'$ where the tile T has b bonds with A' . At equilibrium, the principle of detailed balance tells us that¹²

$$\frac{[A]}{[A'][T]} = \frac{k_f}{k_r} \quad \text{thus} \quad \frac{[A]}{[A']} = \frac{k_f[T]}{k_r} = \frac{r_f}{r_{r,b}} = e^{-(G_{mc} - bG_{se})}.$$

Calculating equilibrium concentrations from any order of tile addition steps yields the same result, so we can calculate the concentration of $A = T_1 T_2 \cdots T_n$ from any sequence of additions for producing A . Let b_i be the number of bonds for the addition



and let $b_A = \sum_{i=1}^{n-1} b_i$ be the total strength of all matching edges in the aggregate. Then,

$$\begin{aligned} \frac{[A]}{[T]} &= \frac{[T_1 \cdots T_n]}{[T_n]} = \frac{[T_1 \cdots T_n]}{[T_2 \cdots T_n]} \frac{[T_2 \cdots T_n]}{[T_3 \cdots T_n]} \cdots \frac{[T_{n-1} \cdots T_n]}{[T_n]} \\ &= e^{-(G_{mc} - b_1 G_{se})} e^{-(G_{mc} - b_2 G_{se})} \cdots e^{-(G_{mc} - b_{n-1} G_{se})} \\ &= e^{-((n-1)G_{mc} - b_A G_{se})} = e^{-((n-1)\mathcal{T} - b_A)G_{se}}. \end{aligned}$$

So we see that the concentrations of aggregates with $\frac{b_A}{n-1} > \mathcal{T}$ will grow with n , while the concentrations of other aggregates will shrink¹³. We would like to make a prediction for error rates based on the equilibrium assumption. To do this, we ignore the total concentration, and just ask, ‘‘Of all material containing size n aggregates, what fraction is without errors?’’

To compute this, we must know the value of b_A for aggregates of interest. Note that for the Sierpinski Tiles, any aggregate A_0 produced by the Tile Assembly Model at $\mathcal{T} = 2$ (i.e., an aggregate with 0 errors) has exactly $b_{A_0} = 2(n-1)$ because every tile addition step contributes

¹¹To account for the possibility that the Tile Assembly Model produces many distinct aggregates, we note that the probability that a size- n aggregate produced by the Kinetic Assembly Model is not also produced by the Tile Assembly Model is exponentially low.

¹²Note that r_f is constant because all monomer concentrations are equal and held constant, while $r_{r,b}$ depends on b for the particular reaction.

¹³Recall that we are assuming equilibrium has been reached; taken literally, this is patently absurd when at equilibrium the concentrations of aggregates grows exponentially with their size. The implication is that in order to hold the monomer concentrations constant, we must continually be providing new material into the system; this new material flows through the system to create larger and larger aggregates.

exactly 2 bonds. Furthermore, all other aggregates must have $m \doteq 2(n-1) - b_A > 0$, a measure of their suboptimality¹⁴. Aggregates with small m look like perfect Sierpinski aggregates, but with a few internal errors. For size n aggregates, one perfect and one suboptimal by m ,

$$\frac{[A_m]}{[A_0]} = \frac{e^{-((n-1)\mathcal{T} - b_{A_m})G_{se}}}{e^{-((n-1)\mathcal{T} - b_{A_0})G_{se}}} = e^{-mG_{se}}.$$

This at least partly explains the absence of aggregates seeded by rule tiles: any aggregate consisting entirely of rule tiles must have $m \geq 2\sqrt{n} - 2$, and thus their equilibrium concentrations are exceedingly low¹⁵.

To compute the fraction of all size- n material which is errorless, we must know *how many* aggregates of each kind there are. Let n_m be the number of distinct size n aggregates of suboptimality m . Then a size n aggregate chosen from the equilibrium distribution is errorless with probability

$$\Pr_{eq}(\text{errorless aggregate}|n) = \frac{n_0[A_0]}{\sum_{m=0}^{\infty} n_m[A_m]} = \frac{1}{\sum_{m=0}^{\infty} \frac{n_m}{n_0} e^{-mG_{se}}}.$$

For small m , we can estimate $\frac{n_m}{n_0}$ by noting that for each perfect aggregate of size n , we can make $\approx \binom{2n}{m}$ suboptimal aggregates by inducing errors at m internal edges, and completing the rest of the pattern properly. Thus,

$$\Pr_{eq}(\text{errorless aggregate}|n) \approx \frac{1}{\sum_{m=0}^{\infty} \binom{2n}{m} e^{-mG_{se}}} = \frac{1}{(1 + e^{-G_{se}})^{2n}} \approx 1 - 2ne^{-G_{se}}.$$

We can see that $\Pr_{eq}(\text{errorless aggregate}) \approx \frac{1}{e}$ at $n = \frac{1}{2}e^{G_{se}}$. Since the G_{se} is determined by the length of sticky ends, we see that by increasing sticky end length, we can exponentially increase the size over which errorless computation can be expected to occur.

We could have arrived at the same conclusion more simply, but less rigorously, by assuming that all tile additions occur in slots and the tile is chosen independently from the local equilibrium distribution. (A site is in *local equilibrium* when the tiles (or their absence) at neighboring positions do not change, and all tile addition and tile dissociation reactions involving the site are in equilibrium.) Then,

$$\Pr_{eq}(\text{errorless aggregate}|n) \approx \Pr_{eq}(\text{errorless step})^n \approx \left(\frac{1}{1 + 2e^{-G_{se}}} \right)^n \approx 1 - 2ne^{-G_{se}}.$$

¹⁴This can be seen by noting that $b_A \leq 2\#(\text{rule tiles} + \text{corner tiles}) + 2.5\#(\text{boundary tiles})$ where the deficit is due to internal mismatches and to the ‘‘surface energy’’ of unmatched edges on the perimeter. An aggregate consisting exclusively of n rule tiles will have perimeter at least $4\sqrt{n}$, and thus $b_A \leq 2n - 2\sqrt{n}$ and $m \geq 2\sqrt{n} - 2$. An aggregate with $g + 1$ boundary and corner tiles will have 2 mismatched or unmatched edges terminating the boundary line and on the perimeter at least g unmatched edges; thus $m \geq 0$.

¹⁵The concentration of a rule tile aggregate A_r is bounded by $[A_r]/[T] \leq e^{(\mathcal{T} + \epsilon n - 2\sqrt{n})G_{se}}$, which has a minimum of $[A_r]/[T] \leq e^{(\mathcal{T} - 1/\epsilon)G_{se}}$ at $n_{critical} = \epsilon^{-2}$. (Recall that $\mathcal{T} = 2 - \epsilon$.) The concentration at the critical size, which becomes a kinetic barrier to the formation of larger aggregates (Erickson 1980), approaches zero as $\mathcal{T} \rightarrow 2$.

Note that this analysis, based on assumptions of equilibrium, predicts that error rates are unaffected by G_{mc} . This was not the result of our simulation: error rates increase dramatically as G_{mc} drops below the melting transition (i.e., as monomer concentration increases). Consequently, we conclude that equilibrium is *not* achieved in these cases.

The kinetic trap. What prevents the system from achieving equilibrium? The intuition is that if the growth of the crystal is faster than the time required to locally establish equilibrium at the growth sites, tiles will become embedded and “frozen” in the interior of the aggregate with an out-of-equilibrium distribution.

How long does it take for a growth site to reach local equilibrium? Consider a growth site that has just formed, and assume that the local context (neighboring tiles) does not change. Monomer tiles of all kinds will sit down at the site, stay a while, and then leave, each according to its own off-rate. If we look immediately after the growth site appears, the probability that the site is empty is near 100%; however, if we wait a very long time before looking, we will find each tile, or an empty site, with their equilibrium probabilities. If the local context *does* change by addition of tiles surrounding the growth site, then the tile currently in place can be “frozen” there effectively permanently; even if it has one mismatched edge, three matches on its other edges can make its off-rate very low. Although this is a very cartoonish picture, it is the basis for our analysis, since the full system is too complex to treat rigorously.

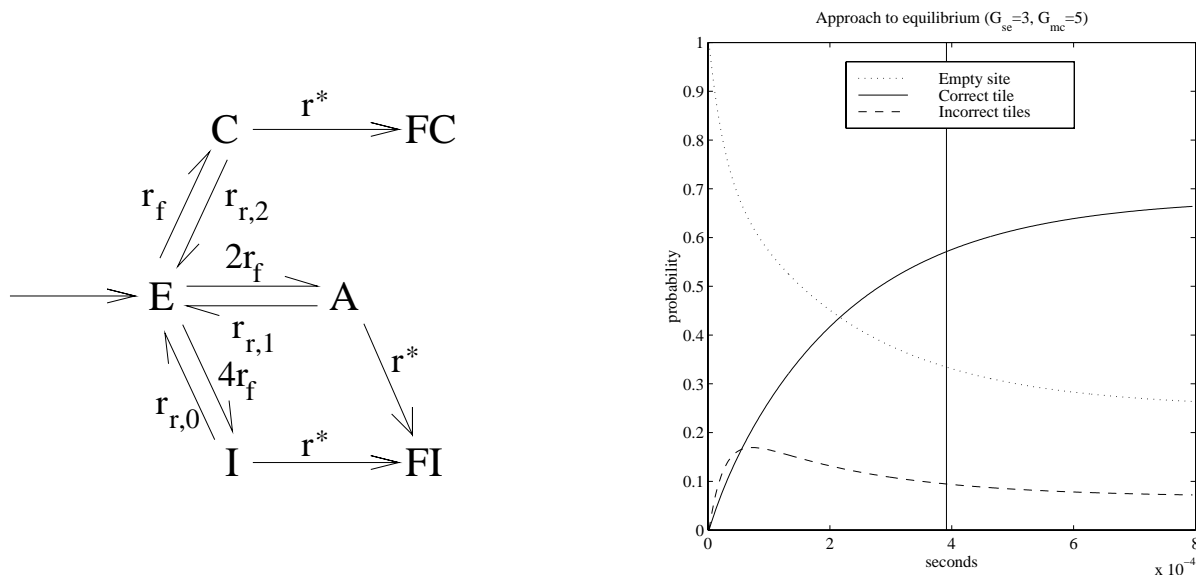


Figure 8: Model for kinetic trapping at a single growth site. (a) Simplified model for the filling of a new site. In state E the site is empty; in state C a correct tile is present; in state A an almost correct tile (with one mismatch) is present; and in state I a tile with several mismatches is present. The sinks FC and FI represent frozen correct tiles and frozen incorrect tiles, respectively. (b) The approach to equilibrium distribution at the site, assuming the site has not yet been frozen. The vertical bar marks the expected time at which the site will be frozen.

Let’s look at the probability of a particular tile being present in the site as a function of time, prior to the site being frozen. For the Sierpinski Tiles, four cases must be distinguished: (E) The site is empty. The “off-rate” of emptiness is $7r_f = 7k_f e^{-G_{mc}}$, since there are 7 tiles. (C)

The correct tile is in place. It's off-rate is $r_{r,2} = k_f e^{-2G_{se}}$. (A) One of two tiles with just one match, and off-rate $r_{r,1} = k_f e^{-G_{se}}$. (I) One of 4 tiles with no matches, and off-rate $r_{r,0} = k_f$. Let $p_i(t)$ be the probability that (i) is the case t seconds after the growth site has appeared, assuming the site has not yet been frozen. The rate equations for the model in Figure 8a, excluding the sinks FC and FI , can be written as

$$\dot{\mathbf{p}}(t) = \begin{bmatrix} -7r_f & r_{r,2} & r_{r,1} & r_{r,0} \\ r_f & -r_{r,2} & 0 & 0 \\ 2r_f & 0 & -r_{r,1} & 0 \\ 4r_f & 0 & 0 & -r_{r,0} \end{bmatrix} \begin{bmatrix} p_E(t) \\ p_C(t) \\ p_A(t) \\ p_I(t) \end{bmatrix} \doteq M\mathbf{p}(t)$$

and thus, $\mathbf{p}(t) = e^{Mt}\mathbf{p}(0)$ where $\mathbf{p}(0) = [1 \ 0 \ 0 \ 0]^T$.

The behavior of $\mathbf{p}(t)$ is shown in Figure 8b. We want to know the probability that the correct tile is in place when the site is frozen. During controlled growth, the rate of growth is approximately $r^* = r_f - r_{r,2}$; thus a given site will be frozen in mean time approximately $t^* = 1/(r_f - r_{r,2})$. With a decrease in G_{mc} (increased monomer concentration), r_f increases, and t^* becomes earlier, leading to a more out-of-equilibrium frozen distribution.

By including sink states FC and FI into the model of Figure 8a, we can solve exactly for the frozen distribution. In this case the equations are

$$\dot{\mathbf{p}}(t) = \begin{bmatrix} -7r_f & r_{r,2} & r_{r,1} & r_{r,0} & 0 & 0 \\ r_f & -r_{r,2} - r^* & 0 & 0 & 0 & 0 \\ 2r_f & 0 & -r_{r,1} - r^* & 0 & 0 & 0 \\ 4r_f & 0 & 0 & -r_{r,0} - r^* & 0 & 0 \\ 0 & r^* & 0 & 0 & 0 & 0 \\ 0 & 0 & r^* & r^* & 0 & 0 \end{bmatrix} \begin{bmatrix} p_E(t) \\ p_C(t) \\ p_A(t) \\ p_I(t) \\ p_{FC}(t) \\ p_{FI}(t) \end{bmatrix} \doteq M\mathbf{p}(t)$$

where $\mathbf{p}(0) = [1 \ 0 \ 0 \ 0 \ 0 \ 0]^T$. The probability of the site being frozen with the correct tile, $p_{FC}(\infty)$, can be easily computed from the steady-state of the related flow problem, where a unit amount of material is pumped into state E and accumulates differentially in FC and FI :

$$\dot{\mathbf{p}}(\infty) = [1 \ 0 \ 0 \ 0 \ p_{FC}(\infty) \ p_{FI}(\infty)]^T = M\mathbf{p}(\infty).$$

A little algebra gives the probability of an errorless step in terms of G_{se} and G_{mc} :

$$\Pr_{kin}(\text{errorless step}) \doteq p_{FC}(\infty) = \frac{\frac{1}{r^* + r_{r,2}}}{\frac{1}{r^* + r_{r,2}} + \frac{2}{r^* + r_{r,1}} + \frac{4}{r^* + r_{r,0}}}.$$

In this equation for errors due to kinetic trapping, in contrast to the equilibrium prediction, the error rate depends upon *both* G_{se} and G_{mc} . The equation predicts error rates that are in qualitative agreement with the simulations, as shown in Figure 9. In this analysis, it becomes clear that in the limit as $\mathcal{T} \rightarrow 2$ and thus $r^* \rightarrow 0$,

$$\Pr_{kin}(\text{errorless step}) \rightarrow \Pr_{eq}(\text{errorless step}) = \frac{1/r_{r,2}}{1/r_{r,2} + 2/r_{r,1} + 4/r_{r,0}} \approx \frac{1}{1 + 2e^{-G_{se}}}.$$

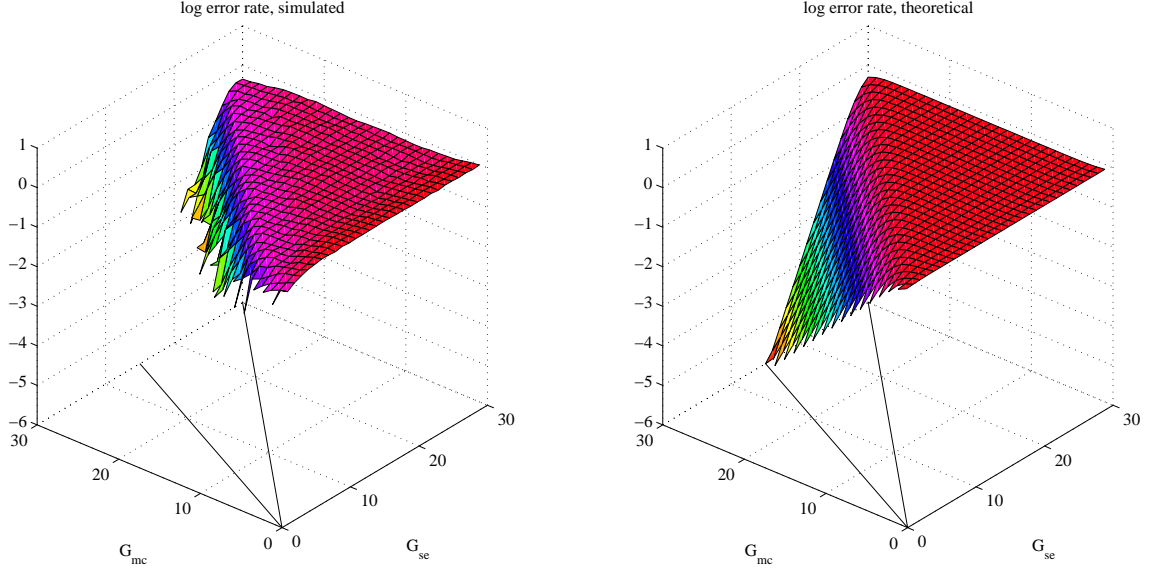


Figure 9: (a) Log_{10} per-step error rates, estimated from simulations. (b) Log_{10} per-step error rates, according to the kinetic trap theory.

Thus equilibrium error rates are achieved near $\mathcal{T} = 2$.

Speed of assembly. We have already observed that the forward rate $r_f = \hat{k}_f e^{-G_{mc}}$ depends upon monomer concentration, and consequently, as our error rates improve with increased G_{mc} , simultaneously the speed of computation drops dramatically. Now that we have an analytical expression for $\text{Pr}_{kin}(\text{errorless step})$, based upon our simplified kinetic trap model, we can determine the conditions which achieve a given target error rate ε with the fastest rate of assembly $r^* = r_f - r_{r,2}$:

$$1 - \varepsilon = \text{Pr}_{kin}(\text{errorless step}) \approx \frac{1}{1 + 2 \frac{r^* + r_{r,2}}{r^* + r_{r,1}}}$$

and thus for small ε and $2G_{se} > G_{mc} > G_{se}$,

$$\varepsilon \approx 2 \frac{r^* + r_{r,2}}{r^* + r_{r,1}} \approx 2e^{-(G_{mc} - G_{se})} \doteq 2e^{-\Delta G}.$$

To achieve error rate ε , the system can be run anywhere along a line parallel to $\mathcal{T} = 1$ but displaced by $\Delta G = \ln 2/\varepsilon$ above it. Where along this line does self-assembly proceed most rapidly? We find the maximum of

$$r^* = \hat{k}_f (e^{-G_{mc}} - e^{-2G_{se}}) = \hat{k}_f (e^{-\Delta G - G_{se}} - e^{-2G_{se}})$$

by differentiation with respect to dG_{se} ; optimal growth for constant ΔG occurs at

$$G_{se} = \Delta G + \ln 2 = \ln \frac{4}{\varepsilon} \quad \text{and} \quad G_{mc} = 2\Delta G + \ln 2 = \ln \frac{8}{\varepsilon^2}.$$

The optimal growth rate $r^* = \frac{\hat{k}_f}{16} \varepsilon^2 \approx 0.75 \times 10^6 \varepsilon^2 / \text{sec}$ occurs on the line $G_{mc} = 2G_{se} - \ln 2$.

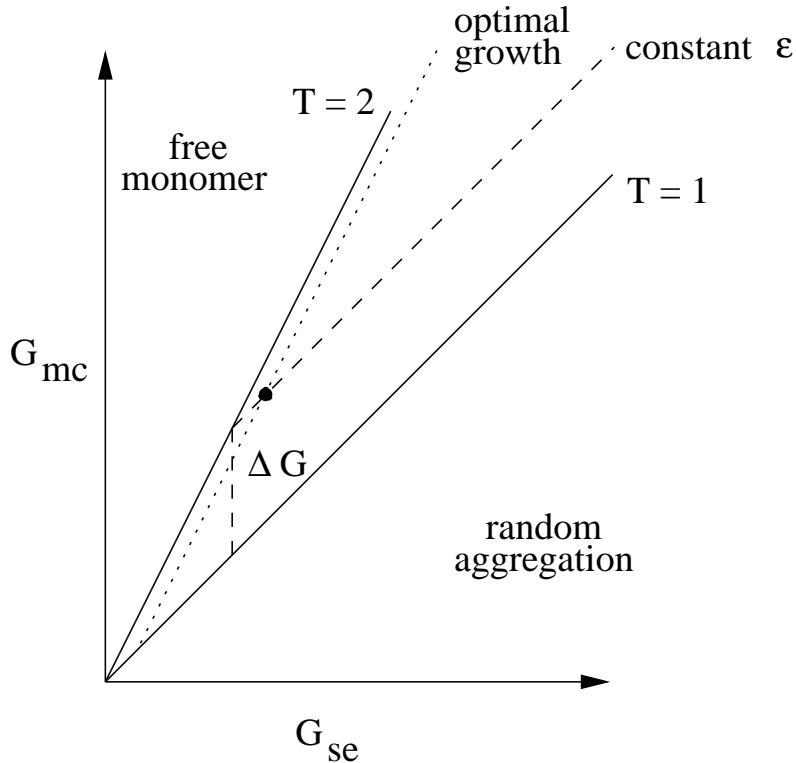


Figure 10: Analysis of the phase diagram for 2D self-assembly. Lines mark the melting transition $\mathcal{T} = 2$, the precipitation boundary $\mathcal{T} = 1$, a line of constant error rate $G_{mc} = G_{se} + \Delta G$, and the line on which optimal growth rates occur $G_{mc} = 2G_{se} - \ln 2$.

Thus it appears that we have a hard physical limit on what error rates can be achieved by DNA self-assembly within reasonable time limits. If we wish to have a net forward rate of 1 tile added per second, then the best we can achieve is an error rate of 1/1000; while if we were willing to wait half an hour for each addition, we could get an error rate of 3×10^{-5} , and we could grow some perfect 200×200 aggregates over the course of a week.

7 Discussion

The above simulations and theoretical arguments both confirm that in the Kinetic Assembly Model, aggregates can grow with finite speed and arbitrarily low per-site error rates for large G_{se} and $\mathcal{T} = 2 - \epsilon$. We should be careful that the analysis does not depend upon the particularities of the Sierpinski Tiles. It can easily be verified that if the rule tiles use k labels (instead of the 2 labels used in the Sierpinski Tiles) and there are a total of N tiles (instead of the 7 Sierpinski Tiles) then the analysis is unchanged except that

$$\text{Pr}_{eq}(\text{errorless aggregate}|n) \approx 1 - 2(k-1)ne^{-G_{se}}$$

and

$$\text{Pr}_{kin}(\text{errorless step}) = \frac{\frac{1}{r^*+r_{r,2}}}{\frac{1}{r^*+r_{r,2}} + \frac{2(k-1)}{r^*+r_{r,1}} + \frac{N-1-2(k-1)}{r^*+r_{r,0}}} \approx 1 - 2(k-1)e^{-(G_{mc}-G_{se})}$$

and the optimal growth rate now occurs displaced $\Delta G = \frac{\ln 2(k-1)}{\epsilon}$ above $\mathcal{T} = 1$. We now loosely discuss other aspects of the model.

Energy use. Reversible computers have the potential to compute using arbitrarily little energy per step, because no information is erased during the computation itself (Landauer 1961; Bennett 1973). The system described here uses only fully physically reversible reactions, and thus is a candidate for low-energy computation; although non-reversible 1D cellular automata may be simulated, the 2D pattern records a history of the entire computation, and thus no information is lost at any step. During controlled growth at $\mathcal{T} = 2 - \epsilon$, the amount of energy used by the system equals the free energy lost as heat on each step:

$$-\Delta G^\circ = -(G_{mc} - 2G_{se})RT = \epsilon G_{se}RT.$$

For any fixed G_{se} , error rates and energy use are simultaneously minimized as the melting transition is approached.

An entropic ratchet. What happens at $\mathcal{T} = 2$ exactly? We already know that at $\mathcal{T} = 2$, optimal equilibrium error rates are achieved and no energy is used to power each step; the probability of going backwards is identical to the probability of going forwards. In a 1D reversible computation, like that imagined by Bennett (1973), the random walk would lead to no net computation performed. However, in our 2D system, the number of possible errorless size n aggregates grows with n . Thus, as the state-space is explored at equilibrium, it will be entropically driven to perform computation! This oddity deserves further attention to see whether it would still be present in a more realistic model.

Experimentally accessible regimes. We have already developed the relation between our abstract parameters G_{mc} and G_{se} and relevant parameters of a real system, such as monomer concentration and free-energies of hybridization; Figure 5 showed that low error rates can be achieved for realistic parameters¹⁶, given our assumptions. We can make our arguments more realistic by considering what happens as a solution of monomers is slowly annealed from a high temperature to a lower temperature. At any moment in time, we plot the current reaction conditions as a point on Figure 6 to determine the rate of growth and per-step error rate. Suppose initially $G_{mc} = 12$ and $G_{se} = 5$; here, above the melting transition, the monomers are all free in solution. As the temperature decreases, G_{se} will increase, and our point follows a horizontal trajectory straight toward $\mathcal{T} = 2$. Just below the melting transition, the aggregate will grow (with optimal error rates for the current G_{se}). Consequently, the monomer concentration will drop, and G_{mc} will increase, bringing the system back toward $\mathcal{T} = 2$. So long as the temperature drops slowly enough, the system will stay just below the melting transition, and our point will follow a trajectory parallel to $\mathcal{T} = 2$. Thus, by annealing, the self-assembly process will automatically maintain itself in the regime where errors are most infrequent. Optimal annealing

¹⁶ $G_{mc} = 30$ is an example of an unrealistic parameter: at 2 pM, $r_f = 2 \times 10^{-5}$ /sec and monomer addition will occur only twice per day.

schedules are an issue for future investigation, and to be of practical use they will have to take account of the non-idealities of the system.

Imperfections of a real system. The careful reader will immediately observe that the concentrations of different tiles will be depleted at different rates, thus breaking our original assumption that all tiles are present at equal concentrations. This will introduce additional factors into the error analysis. There are many other ways in which real systems will deviate from the Kinetic Assembly Model. Free energies of hybridization for different sticky-end sequences cannot be perfectly matched, so the melting transitions for different tiles will differ slightly. Worse yet, imperfectly or partially matched sticky-ends may contribute to the free energy of interaction between tiles with mismatched edges, in violation of the model’s assumption that only correctly edges contribute to $\Delta G_{b,s}^\circ$. It remains to be determined how important these factors are.

Cooperativity of binding. The Kinetic Assembly Model makes a strong assumption that two binding sites on the same tile will act cooperatively when binding to an aggregate. Specifically, it is claimed that $\Delta G_{2\ bonds}^\circ = 2\Delta G_{1\ bond}^\circ$. There are three points to make. First, the rigidity of double crossover molecules, as demonstrated by Li et al. (1996), suggests that the binding events should act together – in particular, the slot-filling event during proper growth should be cooperative. This intuition can be bolstered by estimating the “effective” local concentration of the remaining sticky end after one end has bound – giving an estimate for the additional “loop entropy” (Cantor and Schimmel 1980, p. 1205) required to close the second end in the slot. Since double-stranded DNA has a persistence length of approximately 130 nt (Cantor and Schimmel 1980, p. 1033) and DX molecules span roughly 40 nt from end to end, the physical distance between the sticky ends may fluctuate from 12 to 14 nm, thus exploring a volume of $\approx 4000\text{ nm}^3$, with the free sticky end assuming perhaps a range of $30^\circ \times 30^\circ$ orientations at each position. This corresponds to an effective concentration of

$$C_{eff} = \frac{1\ \text{sticky end}}{4000\ \text{nm}^3 \times 900\ \text{deg}^2} \frac{(10^{24}\ \text{nm}^3 \times 360^2\ \text{deg}^2) / \text{liter}}{6 \times 10^{23}\ \text{sticky ends/mol}} = 60\ \text{mM}$$

and thus a loop entropy $\Delta S_{loop} = R \ln C_{eff} = -5.6\ \text{cal/mol/K}$. This value is comparable with the initiation entropy of $\Delta S_{init} = -6\ \text{cal/mol/K}$. At 27°C it increases the free energy of interaction by 1.68 kcal/mol, which roughly offsets the contribution of a single base-pair bond (−1.4 kcal/mol). The deviation from perfect cooperativity should be negligible, according to this estimation. Experimental studies should be able to measure the extent of cooperativity; the preliminary experiment reported in Winfree et al. (in press) argues qualitatively for cooperativity in an analogous DNA system.

Second, it is possible that in addition to free energy due to sticky end hybridization and due to loop entropy, there could be enthalpic contributions to loop closure, for example, if the double helix must be twisted, stretched, or otherwise deformed in order to fit into the slot. Double crossover molecule tiles can be designed with the intention of minimizing these anticooperative effects, but it remains to be seen how well that works. It may also be possible to *exploit* anticooperative effects to enforce *negative interactions* for mismatching edge labels. This would require using differently sized double crossover molecules, for example by changing the lengths of the four arms, so that geometric mismatches are present in addition to sticky-end sequence

mismatches. It may be possible this way to implement a tile assembly model with negative weights.

Third, just as the initiation entropy was folded into the abstract G_{mc} and G_{se} parameters, a loop entropy or mild anticooperative adjustment could be taken up by adjusting G_{mc} and G_{se} to reproduce the on-rates and off-rates for the most important double-match and single-match cases. The simple model would be inaccurate for the off-rates of tiles with more than 2 bonds, but as these tiles seldom dissociate for parameters of interest, this inaccuracy is irrelevant.

Alternative reaction mechanisms. The Kinetic Assembly Model assumes that the growth of aggregates occurs by addition of single monomers only, and thus that there are no interactions between aggregates. Reaction mechanisms would not affect the equilibrium error rate predictions, but Rothmund (personal communication) has emphasized that dimer-dimer pathways, or other interactions between aggregates, could be very important for the kinetics of self-assembly, and thus their inclusion could affect kinetic trapping in theory and in practice. Indeed, Malkin et al. (1995) have directly observed, by AFM, crystal growth by sedimentation of small three-dimensional nuclei.

It is also possible – perhaps I should say probably – that alternative reaction mechanisms are present for creating non-planar structures, such as tubes or random three dimensional networks. Indeed, experimental studies attempting to create 2D lattices of DX molecules (Winfree et al. 1998) found, for example, occasional unexpected rod-like structures in addition to the expected planar 2D crystals.

8 Conclusions

We have used a pair of simple kinetic models to understand error rates in the self-assembly process for algorithmically-defined 2D polymerization. Our results lend credence, in lieu of a full experimental demonstration, to proposals (Winfree 1996; Winfree et al. in press) for computation by self-assembly of DNA: we have found that 2D self-assembly can theoretically support computation with arbitrarily low error rates. This answers a question raised by Reif (in press), who was concerned that, as in the $\mathcal{T} = 1$ example of Figure 1, an unfortunate sequence of tile additions could lead to *blockages* where no tile can fit into an empty site without a mismatch. We find that blockages are not a problem in our model, but the thermodynamics of DNA hybridization give rise to an intrinsic per-step error rate. Large computations require low concentrations and hence very slow growth rates. This is the algorithmic equivalent of the fact, in conventional crystallization, that large perfect crystals form under conditions of slow growth near the solubility line (Kam et al. 1980).

A few worked-out examples for the case of the Sierpinski Tiles are illustrative. From our investigations of kinetic trapping, we found that there is an optimal growth rate r^* for every target error rate ε . At this growth rate $\varepsilon = 4e^{-G_{se}}$, $[DX] = 2.5\varepsilon^2$ M, and $r^* = 0.75 \times 10^6 \varepsilon^2$ /sec, where $0 < G_{se} = (\frac{4000 \text{ K}}{T} - 11)s \approx -\Delta G^\circ/RT$ for the hybridization of a single sticky end of length s . Assemblies of $n_{max} \doteq 1/\varepsilon$ tiles would be expected to contain one error on average; there is an inverse relationship between the rate of assembly and the expected size of error-free aggregates. For example, sticky ends of length 5 at room temperature give $G_{se} = 12$ and

$n_{max} = 40000$, but requires a concentration of $[DX] = 1.5 \text{ nM}$ and thus a rate $r^* = 1.6$ /hour. The same system could be run at 17°C , where $G_{se} = 14$, $[DX] = 30 \text{ pM}$, $n_{max} = 300000$, and $r^* = 0.71$ /day; or at 45°C , where $G_{se} = 8$, $[DX] = 4.5 \mu\text{M}$, $n_{max} = 750$, and $r^* = 1.35$ /sec. Under the latter conditions, a non-deterministic set of DNA tiles in a reasonable volume (1 ml) could give rise to 10^{13} distinct 300-tile aggregates in under a minute, that is, 10^{14} operations per second. This would be sufficient for solving a simple 40-variable SAT problem by subsequent ligation and PCR to find the answer-containing strand in the “good” aggregate. However, for this application an additional source of errors would be false-positives due to non-answer aggregates which, because of an error during assembly or during PCR, appear to be “good;” an additional error analysis is required in this case.

What are we to do if we want faster and less error-prone computation? Reif (in press) suggests using a combination of autonomous self-assembly and step-wise processing; his ingenious constructions perform a computation in a series of self-assembly steps each of which only requires the formation of small aggregates. Because the number of steps is kept low (for example, computing a circuit of size s requires $O(\log s)$ self-assembly steps), there is promise for asymptotically better error rates; however, a detailed analysis remains to be done, and may be difficult due to the lack of experimental evidence for the complex DNA structures and self-assembly reactions he proposes.

Is it possible to get faster and less error-prone computation in an autonomous self-assembly system? Biology makes use of an energy source to improve error rates by “proofreading” mechanisms (Kornberg and Baker 1991). Kinetic proofreading mechanisms can be fairly simple (Hopfield 1974); it would be interesting if such a mechanism could be devised to mediate the self-assembly of double-crossover molecules. Alternatively, one can accept the intrinsic error rate and try to devise error-correcting *algorithms* which could improve the overall error rate exponentially with a slowdown only linear in the number of extra tile types.

9 Acknowledgements

I am deeply grateful for stimulating discussions, suggestions, questions, and technical help from John Hopfield, Sanjoy Mahajan, Paul Rothemund, Len Adleman, John Reif, and James Wetmur. All errors, whatever their rate may be, are mine.

MATLAB 5.2 code for running the simulations and reproducing all the figures in this paper may be obtained from the author.

This work has been supported by the National Institute for Mental Health (Training Grant # 5 T32 MH 19138-07), General Motors’ Technology Research Partnerships program, and by the Center for Neuromorphic Systems Engineering as a part of the National Science Foundation Engineering Research Center Program (under grant EEC-9402726).

References

Proceedings of the 4th DIMACS Meeting on DNA Based Computers, held at the University of Pennsylvania, June 16-19, 1998, in press .

- Leonard M. Adleman. Molecular computation of solutions to combinatorial problems. *Science*, 266:1021–1024, 1994.
- Charles H. Bennett. Logical reversibility of computation. *IBM Journal of Research and Development*, 17:525–532, 1973.
- Robert Berger. The undecidability of the domino problem. *Memiors of the AMS*, 66:1–72, 1966.
- Michael Biafore. Universal computation in few-body automata. *MIT*, preprint.
- Dan Boneh, Chris Dunworth, Richard J. Lipton, and Jiří Sgall. On the computational power of DNA. *Discrete Applied Mathematics*, 71:79–94, 1996.
- Charles R. Cantor and Paul R. Schimmel. *Biophysical Chemistry, Part III: The behavior of biological macromolecules*. W. H. Freeman and Company, 1980.
- H. P. Erickson. Self-assembly and nucleation of a two-dimensional array of protein subunits. In *Electron Microscopy at Molecular Dimensions*, pages 309–317. Baumeister & Vogell, 1980.
- Tsu-Ju Fu and Nadrian C. Seeman. DNA double-crossover molecules. *Biochemistry*, 32:3211–3220, 1993.
- Branko Grünbaum and G. C. Shephard. *Tilings and Patterns*. W. H. Freeman and Company, New York, 1986.
- Masami Hagiya, Masanori Arita, Daisuke Kiga, Kensaku Sakamoto, and Shigeyuki Yokoyama. Towards parallel evaluation and learning of boolean μ -formulas with molecules. In Wood (in press).
- William Hanf. Nonrecursive tilings of the plane I. *The Journal of Symbolic Logic*, 39:283–285, 1974.
- Alexander J. Hartemink and David K. Gifford. Thermodynamic simulation of deoxynucleotide hybridization for DNA computation. In Wood (in press).
- John J. Hopfield. Kinetic proofreading: a new mechanism for reducing errors in biosynthetic processes requiring high specificity. *Proc. Nat. Acad. Sci. USA*, 71(10):4135–4139, 1974.
- Nataša Jonoska, Stephen A. Karl, and Masahico Saito. Creating 3-dimensional graph structures with dna. In Wood (in press).
- Z. Kam, A. Shaikevitch, H. B. Shore, and G. Feher. Crystallization processes of biological macromolecules. In *Electron Microscopy at Molecular Dimensions*, pages 302–308. Baumeister & Vogell, 1980.
- Arthur Kornberg and Tania A. Baker. *DNA Replication (2nd ed.)*. W. H. Freeman and Company, 1991.

- R. Landauer. Irreversibility and heat generation in the computing process. *IBM Journal of Research and Development*, 3:183–191, 1961.
- Xiaojun Li, Xiaoping Yang, Jing Qi, and Nadrian C. Seeman. Antiparallel DNA double crossover molecules as components for nanoconstruction. *Journal of the American Chemical Society*, 118(26):6131–6140, 1996.
- Richard J. Lipton. DNA solutions of hard computational problems. *Science*, 268:542–544, 1995.
- A. J. Malkin, Yu. G. Kuznetsov, T. A. Land, J. J. DeYoreo, and A. McPherson. Mechanisms of growth for protein and virus crystals. *Nature Structural Biology*, 2(11):956–959, 1995.
- Norman Margolus. Physics-like models of computation. *Physica 10D*, pages 81–95, 1984.
- Dale Myers. Nonrecursive tilings of the plane II. *The Journal of Symbolic Logic*, 39:286–294, 1974.
- Qi Ouyang, Peter Kaplan, Shumao Liu, and Albert Libchaber. DNA solution of the maximal clique problem. *Science*, 278:446–449, 1997.
- Roger Penrose. Pentaplexity. *Eureka*, 39:16–22, 1978.
- Robin S. Quartin and James G. Wetmur. Effect of ionic strength on the hybridization of oliodeoxynucleotides with reduced charge due to methylphosphonate linkages to unmodified oligodeoxynucleotides containing the complementary sequence. *Biochemistry*, 28:1040–1047, 1989.
- John Reif. Local parallel biomolecular computing. In Wood (in press).
- Raphael M. Robinson. Undecidability and nonperiodicity of tilings of the plane. *Inventiones Math.*, 12:177–909, 1971.
- Kensaku Sakamoto, Daisuke Kiga, Ken Momiya, Hidetaka Gouzu, Shigeyuki Yokoyama, Shuji Ikeda, Hiroshi Sugiyama, and Masami Hagiya. State transitions with molecules. In *Proceedings of the 4th DIMACS Meeting on DNA Based Computers, held at the University of Pennsylvania, June 16-19, 1998* 4AW (in press).
- John SantaLucia, Jr., Hatim T. Allawi, and P. Ananda Seneviratne. Improved nearest-neighbor parameters for predicting DNA duplex stability. *Biochemistry*, 35(11):3555–3562, 1996.
- A. R. Smith, III. Simple computation-universal cellular spaces. *Journal of the ACM*, 18:339–353, 1971.
- Paul J. Steinhardt and Stellan Ostlund, editors. *The Physics of Quasicrystals*. World Scientific, Singapore, 1987.
- Hao Wang. Dominoes and the AEA case of the decision problem. In *Proc. Symp. Math. Theory of Automata*, pages 23–55, New York, 1963. Polytechnic Press.

- James G. Wetmur. DNA probes: Applications of the principles of nucleic acid hybridization. *Critical Reviews in Biochemistry and Molecular Biology*, 36:227–259, 1991.
- Erik Winfree. On the computational power of DNA annealing and ligation. In Richard J. Lipton and Eric B. Baum, editors, *DNA Based Computers: Proceedings of a DIMACS Workshop, April 4, 1995, Princeton University*, volume 27 of *DIMACS: Series in Discrete Mathematics and Theoretical Computer Science*, pages 199–221, Providence, RI, 1996. American Mathematical Society.
- Erik Winfree. Whiplash PCR for $O(1)$ computing. In *Proceedings of the 4th DIMACS Meeting on DNA Based Computers, held at the University of Pennsylvania, June 16-19, 1998* 4AW (in press).
- Erik Winfree, Furong Liu, Lisa A. Wenzler, and Nadrian C. Seeman. Design and self-assembly of two-dimensional DNA crystals. *Nature*, to appear, 1998.
- Erik Winfree, Xiaoping Yang, and Nadrian C. Seeman. Universal computation via self-assembly of DNA: Some theory and experiments. In Laura Landweber and Richard Lipton, editors, *Proceedings of the 2nd DIMACS Meeting on DNA Based Computers, held at Princeton University, June 10-12, 1996*, DIMACS: Series in Discrete Mathematics and Theoretical Computer Science., Providence, RI, in press. American Mathematical Society.
- David Wood, editor. *Proceedings of the 3rd DIMACS Meeting on DNA Based Computers, held at the University of Pennsylvania, June 23-25, 1997*, DIMACS: Series in Discrete Mathematics and Theoretical Computer Science., Providence, RI, in press. American Mathematical Society.